Physica Medica 58 (2019) 131–140

Contents lists available at ScienceDirect

Physica Medica

journal homepage: www.elsevier.com/locate/ejmp

Original paper

Design and implementation of a radiation dose tracking and reporting system for mammography and digital breast tomosynthesis

Bruno Barufaldi[a,*], Homero Schiabel[b], Andrew D.A. Maidment[a]

[a] University of Pennsylvania, Department of Radiology, 3620 Hamilton Walk, Philadelphia, PA 19104, United States
[b] University of Sao Paulo, Department of Electrical Engineering, 400 Trabalhador Sao-Carlense, Sao Carlos, SP 13566-590, Brazil

ARTICLE INFO

Keywords:
DICOM
Digital mammography
Digital breast tomosynthesis
PACs

ABSTRACT

A tracking system has been implemented to monitor radiation dose for digital mammography (DM) and digital breast tomosynthesis (DBT). This system communicates with a PACS through DICOM messages that allow the image metadata to be stored in a relational database. The tracking system accepts X-ray breast images, maps the image metadata into a SQL database, and allows a client-side application to report the data using a business intelligence framework. The database contains the DICOM information of 54,244 studies (235,225 images) acquired from four Selenia Dimensions systems. The average time to receive the images, and then extract and write the metadata into the database is 2.28 s for a DM and 3.84 s for a DBT image. Using the stored metadata, physics reports are generated based on chosen criteria (i.e., system model, mammography unit, breast data, acquisition techniques, physician, etc.). Our results show that the mean average glandular dose (AGD) varies significantly with compressed breast thickness and age. We observed an overall dose increase of 25.6% between DM and DBT (1.76 vs 2.21 mGy).

1. Introduction

Since patient safety is a major concern for radiological health care services [1–4], there has been considerable effort to reduce radiation exposure [5–9], and substantial research has been devoted to developing new approaches to monitor patient radiation dose of computed tomography [1]. In clinical practice, a customized system focused on digital mammography (DM) and digital breast tomosynthesis (DBT) may detect inadvertent radiation overexposures and provide a better understanding of the dosimetric consequences of the various radiation exposure settings.

The current study presents an automated system focused on X-ray breast imaging. The system extracts the image metadata from X-ray breast images, stores these data into a relational database, and uses a client-side reporting application to show the results in real-time. The tracking system was implemented in a clinical institution for screening and diagnostic mammography; at the time of this report, the database contained 54,244 studies (235,225 images). This system has been used to monitor radiation dose in DM and DBT in clinical practice [10–12].

The aim of this study is to present the design of the dose tracking system and to characterize the mammographic acquisition settings used in our institution. This study illustrates the use of the tracking system for generating radiation dose and physics reports. We used this dose tracking system to monitor breast compression, radiation dose, and X-ray technique in a mixed imaging environment with screening and diagnostic mammography (DM and DBT).

2. Method

2.1. System overview

The Digital Imaging and Communications in Medicine (DICOM) standard is an all-encompassing data transfer, storage, and display protocol designed to cover all functional aspects of digital imaging systems [13]. Since images are recorded in accordance with the DICOM standard, they can be transmitted and processed by DICOM devices and software known as application entities (AEs). The AEs establish communication to the Picture Archiving and Communication System (PACS) by exchanging DICOM message service elements (DIMSEs) [13]. The AEs act pairwise as a Service Class Provider (SCP) and a Service Class User (SCU) to communicate. DICOM files from an SCU are transmitted via TCP/IP (Transmission Control Protocol/Internet Protocol) to a SCP when it receives a 'store' DIMSE message (C-STORE).

The tracking system consists of two modules: a custom DICOM SCP and a client-side application that is used in clinical practice to generate physics reports for radiation monitoring in breast imaging (Fig. 1). Both

* Corresponding author.
E-mail addresses: Bruno.Barufaldi@uphs.upenn.edu (B. Barufaldi), homero@sc.usp.br (H. Schiabel), Andrew.Maidment@uphs.upenn.edu (A.D.A. Maidment).

https://doi.org/10.1016/j.ejmp.2019.02.011
Received 23 November 2018; Received in revised form 31 January 2019; Accepted 13 February 2019
Available online 16 February 2019

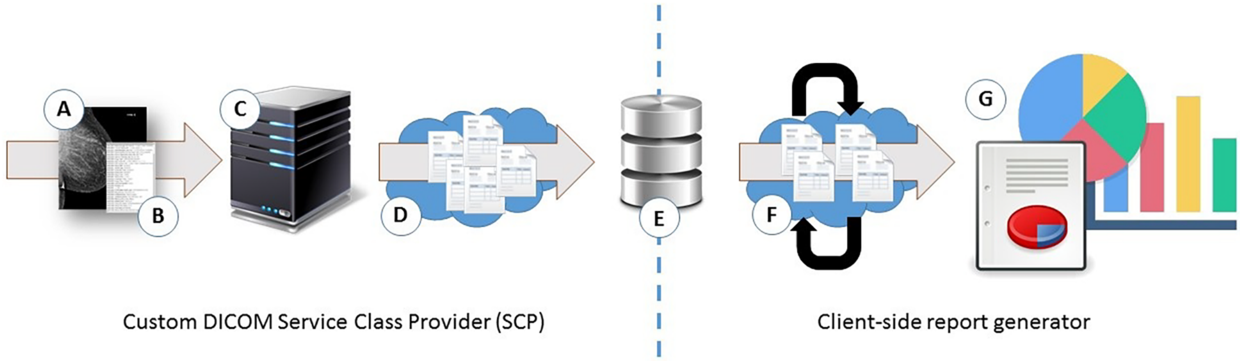

Fig. 1. Tracking and reporting system flow chart. (A) Image and (B) DICOM header are pushed into the server from PACS via TCP/IP (DIMSE C-STORE). The (C) DICOM server, implemented as SCP, extracts (D) the DICOM metadata, and stores into a (E) SQL relational database. (F) The metadata is combined to generate (G) reports for quality assurance and radiation dose monitoring.

modules are interfaced to a structured query language (SQL) database; sharing the exposure information and patient breast data acquired from the PACS.

A SQL database (Microsoft SQL Server 2016, Microsoft Corporation, Redmond, WA) was used to store the image metadata. The DICOM SCP was implemented using C#, the .NET 4.5.2 Framework, the Fellow Oak DICOM 3.0, and Entity Framework 6.1.3 for .NET. This system was developed using a Microsoft Windows Server 2008 R2 64-bit environment equipped with an Intel Xeon 3.4 GHz processor, 32 GB RAM and four 2 TB hard drives.

2.2. Metadata storage

DICOM files contain a file header with patient and study metadata. In the DICOM model [14], a patient has at least one study (i.e. exam or procedure) that consists of series of images and other reported results. A series typically equates to a specific modality or acquisition system, and it contains at least one SOP instance (i.e. images, dose reports, etc.). This hierarchical model is mandatory for any DICOM system, and is designed to support relational data processing.

DICOM headers follow a tagged file format that describes the study and series metadata for a particular patient. This information follows a specific data dictionary [15], and it is frequently parsed and used as indexing data by the PACS. The hierarchical model, which contains the attributes used for our breast health database, is shown in Fig. 2.

To store the information into the relational SQL database, the custom DICOM SCP identifies the conveyed DICOM commands from PACS with DIMSE messages. PACS uses the DIMSE C-FIND, C-MOVE, and C-STORE services exchanged over an established association via TCP/IP.

The C-FIND operation returns a series of SOP instances for each study request. The C-MOVE allows an AE to transfer the stored SOP instances to another AE using the C-STORE command [13]. During the C-STORE request, the custom DICOM SCP accepts the incoming association requests, opens a SQL connection, and parses and stores the metadata from the DICOM headers into the database (Fig. 3). A metadata backup file is created and saved locally on the disk as a secure copy. At our institution, we maintain all metadata in compliance with our IRB approval. This was possible because the database resides within our clinical environment. It would also be possible to anonymize the metadata before being saved in the database, since the accession number and various DICOM unique identifiers (UIDs) provide a cross-reference to the study on the PACS. Our software provides this functionality.

To manipulate the image metadata, relational objects are created for each of the SQL database entities. These objects are responsible for acquiring, validating, normalizing, and updating the database. The activity diagram for the C-STORE process for the PACS and the developed application is shown in Fig. 4.

We are using a client-side report application to access the SQL database and to generate reports. Note that the database access for metadata analysis is independent of the C-STORE processes (Figs. 1 and 3). Database queries can be performed in real-time.

2.3. Client-side report generator

A client-side application is used to retrieve and analyze the stored breast image metadata. This application is an instance of the business intelligence (BI) analytic tool SharePoint Server 2013 (Microsoft Corporation, Redmond, WA), which provides a secure place for storing and tracking image metadata from a customized website.

Since the stored image metadata may be acquired from multiple mammography units located at different sites, it can be difficult to link, match, and transform these data. BI applications allow the manipulation of data acquired from the various external sources, the development and execution of queries against the database(s), and the creation of reports, dashboards and data visualizations (Fig. 1). The data visualization is fast and dynamic, allowing the use of resources such as filters, pivot tables, and charts that make the operation of the mammography systems easier to understand in clinical practice.

The tracking system can illustrate the data using a variety of data visualizations (e.g., radiation dose as a function of breast thickness, as shown in Fig. 5). The data visualization supports different user roles, such as radiologists, technical supervisors, and medical physicists, to improve the decision-making process by presenting the clinical information in different ways.

3. Materials

3.1. Data collection

The image data was provided by the Breast Imaging Center of the University of Pennsylvania Health System (UPHS). This imaging center offers screening and diagnostic DM and DBT, together with other breast imaging services. The institutional review board waived the requirement to obtain written consent for this retrospective, Health Insurance Portability and Accountability Act (HIPAA)-compliant study.

The studies were stored in a Sectra IDS7 PACS (Sectra, Linköping, Sweden). The images were acquired on four Selenia Dimensions systems (Hologic Inc., Bedford, MA), using the following modes: “Conventional”, “Tomo”, “Tomo Combo”, “Tomo Combo HD”, or “Tomo HD”. The Conventional and Tomo modes perform DM and DBT acquisitions, respectively. The Tomo Combo mode acquires DM and DBT acquisitions under the same breast compression, while Tomo HD mode acquires DBT date only and creates a synthetic DM from the DBT data. Finally, the Tomo Combo HD mode acquires DM, DBT, and

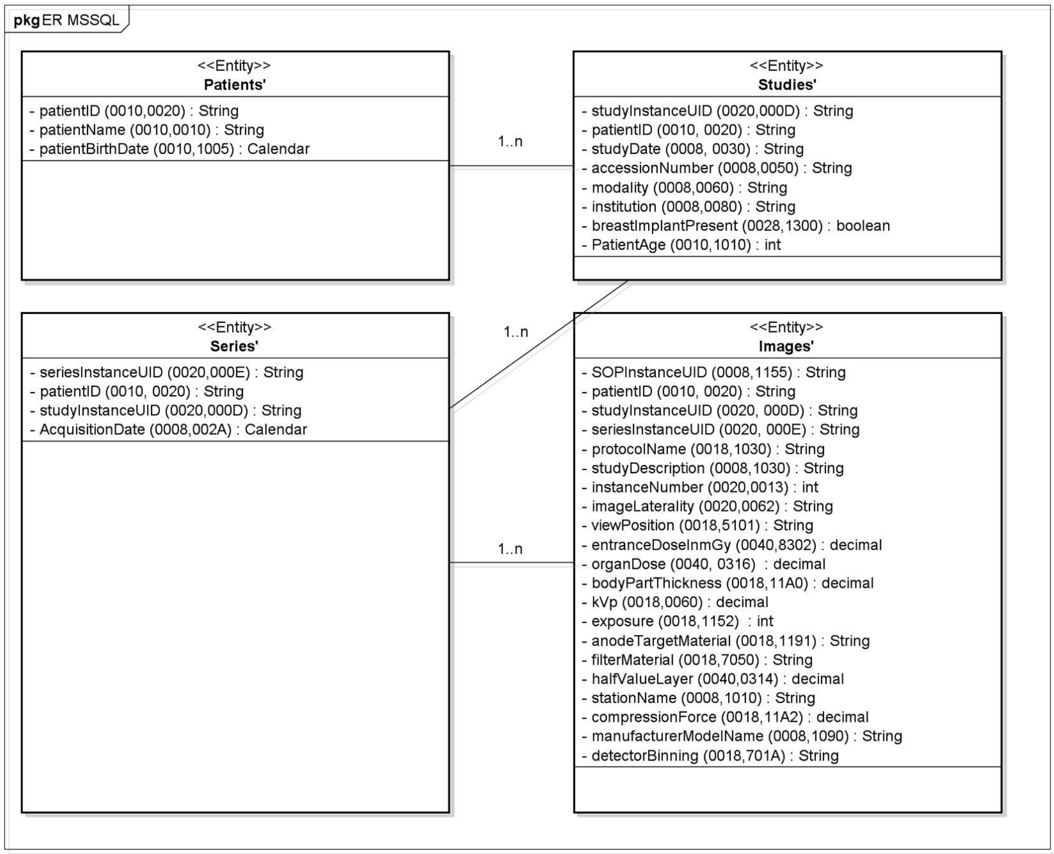

Fig. 2. Entity-relationship diagram for the implemented relational SQL database.

synthetic DM images under the same breast compression. A comparison of acquisition modes is not covered in this work, since this dose information was published previously [12].

In this study, we collected the patient data from our screening population using Conventional, Tomo, and Tomo Combo modes. The screening mammography protocol in our clinical institution requires

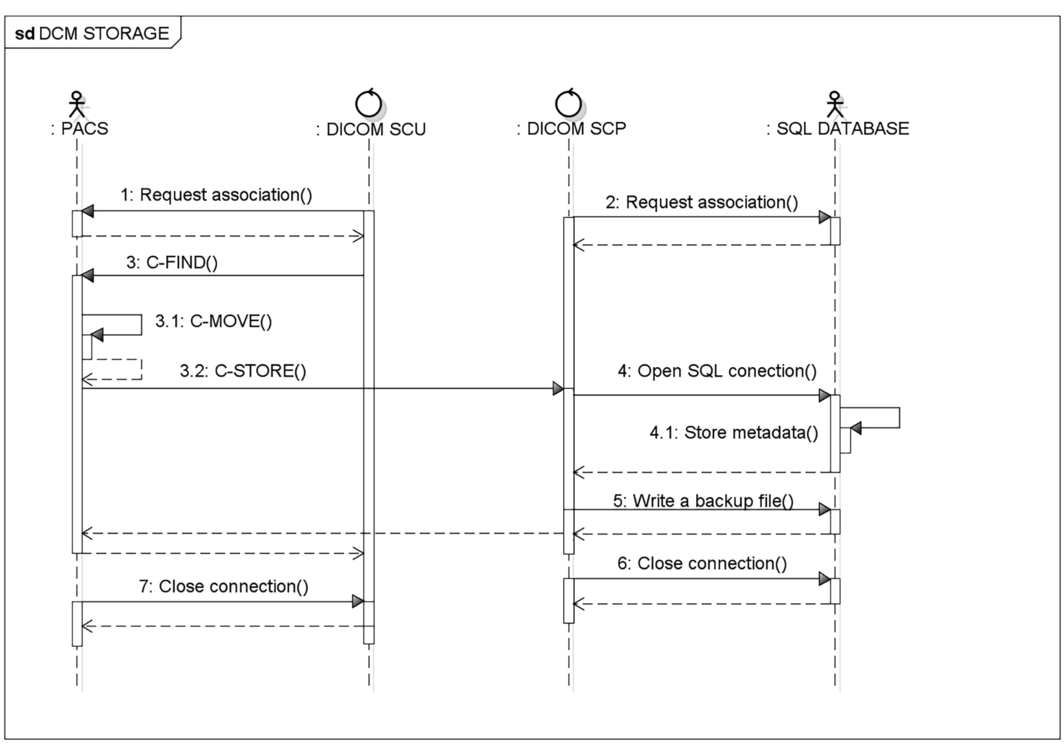

Fig. 3. Sequence diagram for the storage process from PACS to the developed DICOM server.

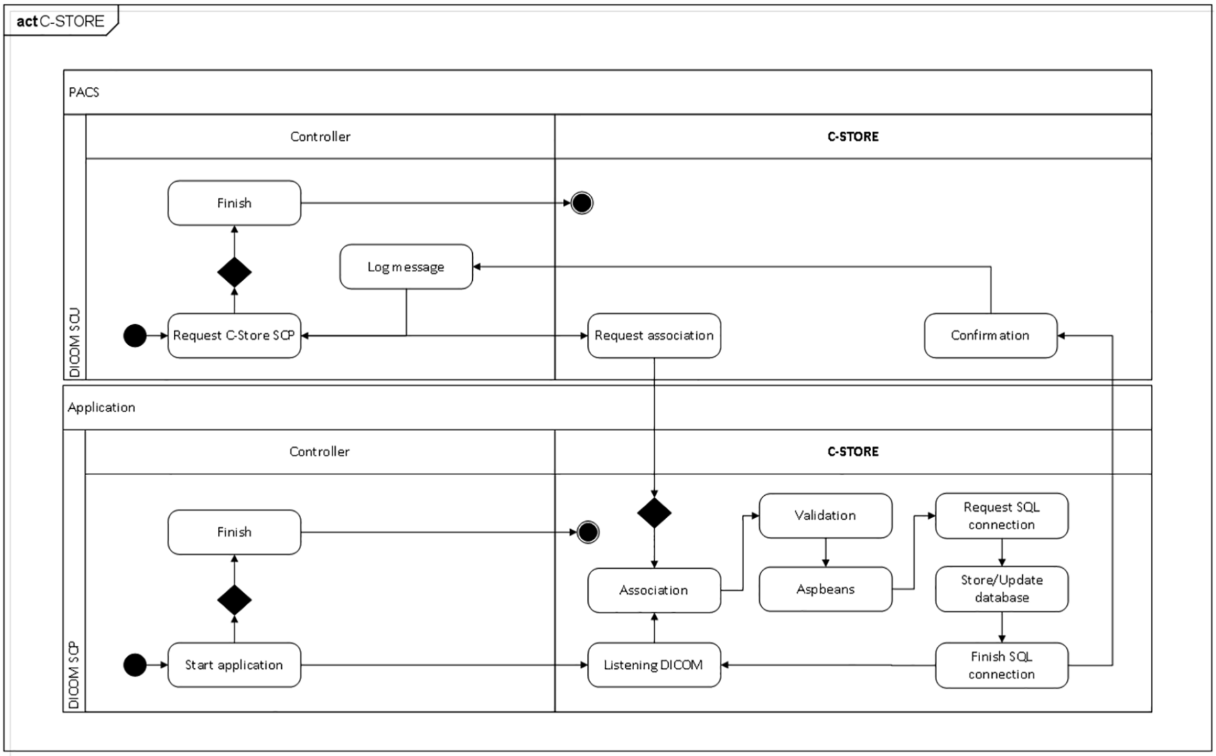

Fig. 4. Activity diagram for the DIMSE C-STORE and metadata storage process.

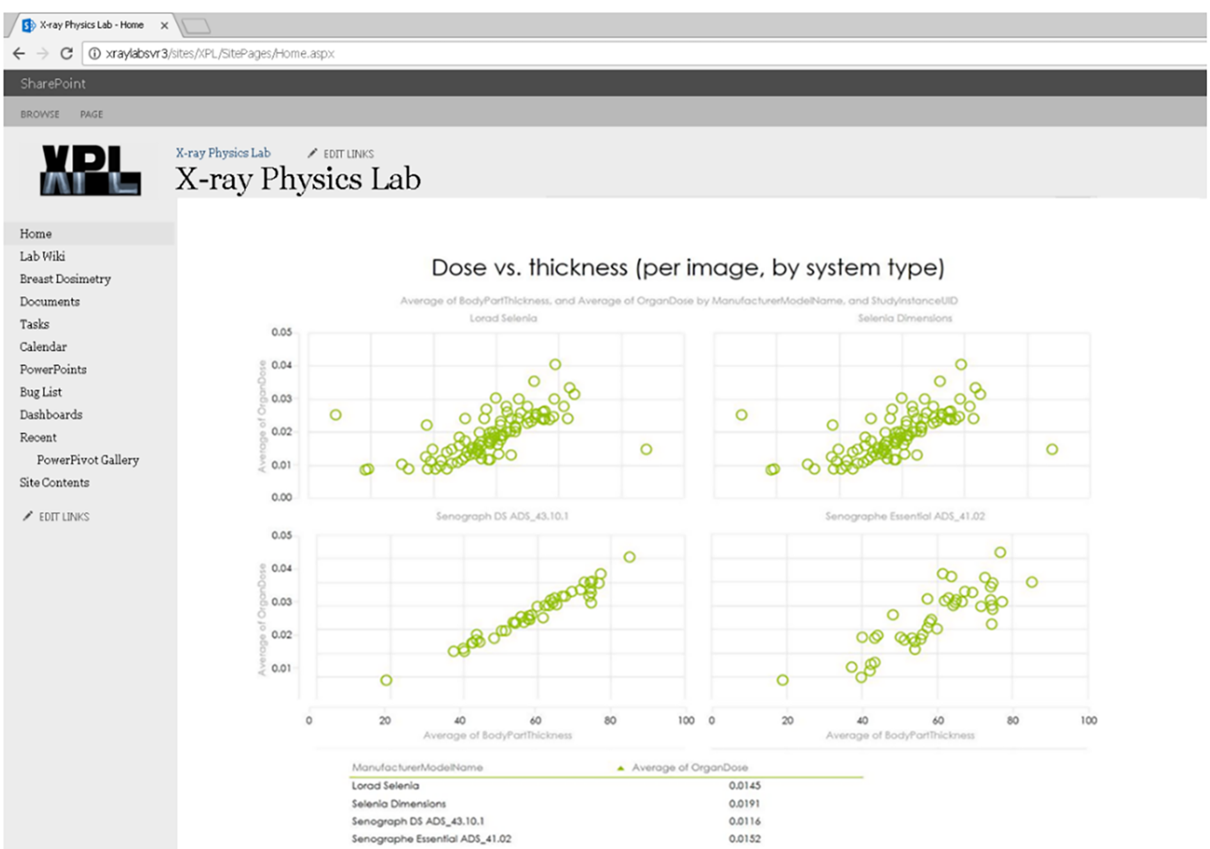

Fig. 5. Example of a web report used to show the clinical breast health data stored in the database.

Table 1
Summary of patient characteristics stratified by breast view, number of images and average compressed breast thickness (CBT).

Modality	No. Studies	Age, years	Breast View (avg ± SD)	No. Images	CBT, mm (avg ± SD)
DM	30,369	56 ± 11	CC	63,046	56.6 ± 13.7
			MLO	75,659	63.3 ± 16.6
			CC & MLO	**138,705**	**60.2 ± 15.7**
DBT	23,875	56 ± 11	CC	47,981	57.2 ± 13.8
			MLO	48,539	63.4 ± 17.1
			CC & MLO	**96,520**	**60.3 ± 15.8**

two images per breast, cranio-caudal (CC) and medio-lateral oblique (MLO). Additional CC and MLO exposures may be needed to address positioning, artifacts, or breast size. Other projections (not CC or MLO) were excluded from the data analysis presented in this work. Automatic exposure control was used for the vast majority of the images. The clinical protocol also allows the use of manual mode for particular cases, such as dense breasts. Manual acquisition was only used in 0.7% of cases. A summary of patient characteristics is shown in Table 1.

3.2. Data analysis

For a trial experiment, we initially stored a set of 100 DM studies and 100 DBT studies that were pushed to the system. From each set, the storage time (DIMSE C-STORE), measured as the time to receive, process and store the metadata, was calculated. Since most of the metadata are duplicated in the raw (“For Processing”) and processed (“For Presentation”) DM images, we extracted and stored the metadata only from the processed images.

The DBT studies include sets of low-dose two-dimensional projection images obtained at different angles. The reconstruction software processes and reconstructs the acquired projections, resulting in sets of reconstructed images (3D breast volume). The DICOM headers contain some duplicate values in the projection and reconstructed images. The patient data was acquired only from the reconstructed DBT image. The patient data from the projections were not saved in the database to avoid duplication. It should be stressed that SQL databases do not allow duplicated primary keys. Because we are using the DICOM hierarchical model [15] and DICOM UID as primary keys, all studies pushed into our system were stored without duplicate entries.

Once the breast information is stored, the client-side reporting system performs analytical operations such as aggregation, drill-down, filtering, and pivoting using the DICOM attributes (i.e. imaging settings, patient information, operator, etc.) defined in the database. Thus, the user can analyze the data in real-time. Reports were generated to analyze various parameters (e.g., compression force, breast thickness, patient age, target-filter combination, kV, etc.) that affect the radiation dose provided by the manufacturer.

The correlation between the parameters that affect radiation dose was assessed by using Pearson’s coefficient (r) because the variables follow normal distributions. The Shapiro-Wilk test was calculated (W) to verify that the variables are normally distributed (testing against the assumption of normality). The analysis of variance (ANOVA) and t-test were used to test differences between means of the categorical variables that follow normal distributions. The non-parametric Kruskal-Wallis test by rank and the Mann-Whitney-Wilcoxon (MWW) test were used to compare independent and non-normal distributions, i.e., when the assumptions of ANOVA are not valid.

We used Cohen’s conventions to interpret the correlation of the variables [16]. A correlation coefficient lower than (±)0.30 represents a weak or small association; a correlation coefficient from (±)0.30 to (±) 0.50 is considered a moderate correlation; and a correlation coefficient of (±)0.50 or larger is thought to represent a strong or large correlation.

3.2.1. Breast compression

Technologists should apply breast compression that is both appropriate and tolerable, so that the mammography unit selects correct technique factors. The compression force and compressed breast thickness (CBT) are recorded in the DICOM header. Depending upon the mammography system, this information can either be provided automatically by the manufacturer or entered manually by the technician; in the current study, these data are provided by the manufacturer. We retrieved the compression force information from the SQL database to analyze the force applied to the patients’ breasts. The compression force was analyzed as a function of CBT, patient age, and breast view. The CBT was analyzed as a function of kV and target-filter combination.

3.2.2. X-ray spectrum and radiation dose

The X-ray spectrum is a critical factor for optimization of image quality and radiation dose in breast imaging. The acquisition settings that determine the X-ray spectrum can be selected automatically by the mammography system (i.e., automatic exposure control mode), or by a technician who operates the mammography unit (manual mode). Automatic exposure control (AEC) typically determines the X-ray spectrum by acquiring a very low dose image of the breast, which together with the measured breast thickness can quantify the density of the mammary tissue. Based on this measurement, the mammography system calculates the appropriate acquisition settings for imaging (e.g., the target-filter combination, kV, mAs, etc.), and also calculates an estimate of the patient dose. In the current study, the average glandular dose (AGD) was acquired using information recorded in the DICOM header (tag 0040,0316). We analyzed the AGD as a function of CBT and patient age.

4. Results

4.1. System storage performance

We calculated the storage time for a set of 100 DM studies and 100 DBT studies that were pushed to the dose tracking system (Table 2). The tracking system took 9.44 s and 16.73 s on average to process and store a DM and DBT study, respectively. The storage time varies in accordance with the number and size of images contained in each study. Note that the storage time per kilobyte transferred is the same for both imaging modalities (0.10 ± 0.00 ms). All studies pushed into our system were successfully stored.

4.2. Compression force

In mammography (DM and DBT), the amount of breast compression is one of the factors that determines the exposure settings selected by the AEC. The histograms of compression force for DM and DBT follow

Table 2
Performance simulation for data storage from PACS to DICOM SCP (DIMSE C-STORE) via TCP/IP.

Modality	No. Studies	No. Images	Time per study, s (avg ± SD)	Time per image, s (avg ± SD)	Time per kilobyte, ms (avg ± SD)	Total Time (mm:ss.SSS)
DM	100	414	9.44 ± 5.19	2.28 ± 2.10	0.10 ± 0.00	15:44.116
DBT	100	436	16.73 ± 11.17	3.84 ± 3.69	0.10 ± 0.00	27:53.321

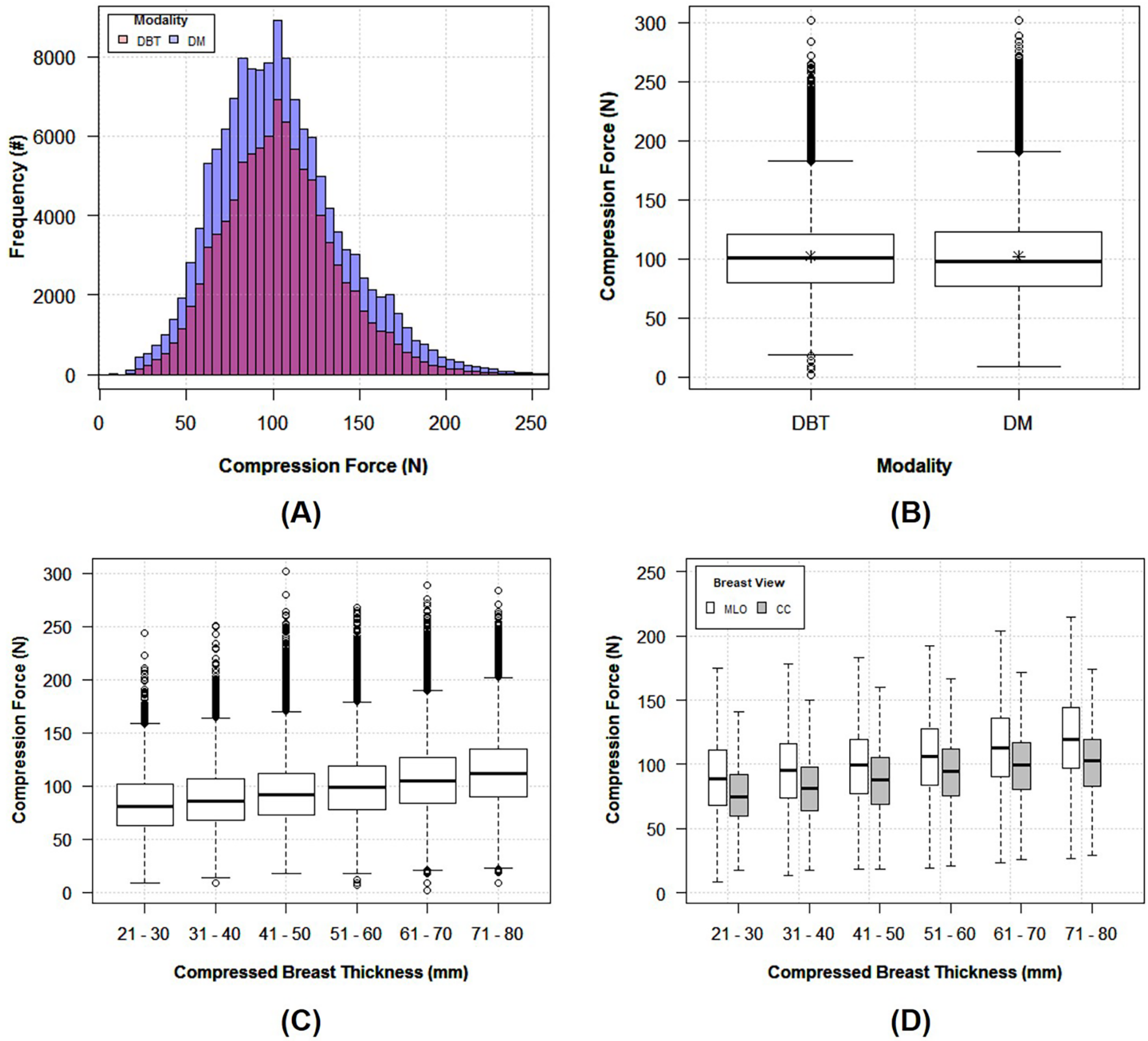

Fig. 6. (A) Histogram and (B) box plot of compression force for DM and DBT images, (C) box plot of compression force as a function of CBT, and (D) box plot of compression force as a function of CBT, stratified by breast view.

similar distributions (Fig. 6A). Both DM and DBT are not normal distributions ($W > 0.7$ and p-value < 0.001).

Fig. 6B shows that there were no significant differences in compression force of DM and DBT images (p-value = 0.68). The average compression force is for both DM and DBT images (102 N). The bottom and top of the box are the 25th and 75th percentile (the lower and upper quartiles, respectively), and the band near the middle of the box is the 50th percentile (the median). The upper and lower whisker represent 1.5 times the interquartile range. The outliers represent the data points located outside the whiskers. Note that the images generated with compression force above 200 N were considered outliers. Our tracking system showed 1,755 (1.3%) DM images and 632 (0.7%) DBT images where the compression force was higher than 200 N. In addition, our tracking system showed 421 (0.3%) DM images and 96 (0.1%) DBT images where there was no compression force information (zeros); note that the Selenia Dimensions typically will not record very low compression force values.

The compression force tends to be higher for thicker breasts (Fig. 6C). A weak positive correlation between CBT and compression force exists (r = 0.26). However, Kruskal–Wallis test by rank showed that there were significant differences in a comparison of categorical CBT values (p-value < 0.001).

On average, the compression force (Fig. 6D) was higher for MLO than CC views; a weak positive correlation between CBT and compression force exists for CC (r = 0.24) and MLO (r = 0.26) views. However, Kruskal–Wallis test by rank showed significant differences in a comparison of categorical CBT values (p-value < 0.001), which vary from 12% to 24% depending upon the CBT.

4.3. X-ray spectrum

Fig. 7A shows the phototimer settings characterized by CBT and target-filter combination for DM; the AEC is typically set to switch the target-filter combination from W/Rh to W/Ag at a CBT of 70 mm. However, we found that 0.71% of the images (713 out of 100,696) were of breasts thicker than 70 mm imaged with W/Rh. Also, we found 0.29% of the images (295 out of 100,696) were of breasts thinner than 70 mm imaged with W/Ag.

For DM, the Selenia Dimensions system usually selects lower kV and W/Rh to acquire images of thinner breasts (Fig. 7B). For thicker breasts, these systems select higher kV and W/Ag. Only 241 images (0.6%) were acquired using the W/Ag target-filter and kV < 29 combination. Similarly, only 230 images (0.2%) were acquired using the W/Rh target filter and kV >34. A strong positive correlation between CBT and kV

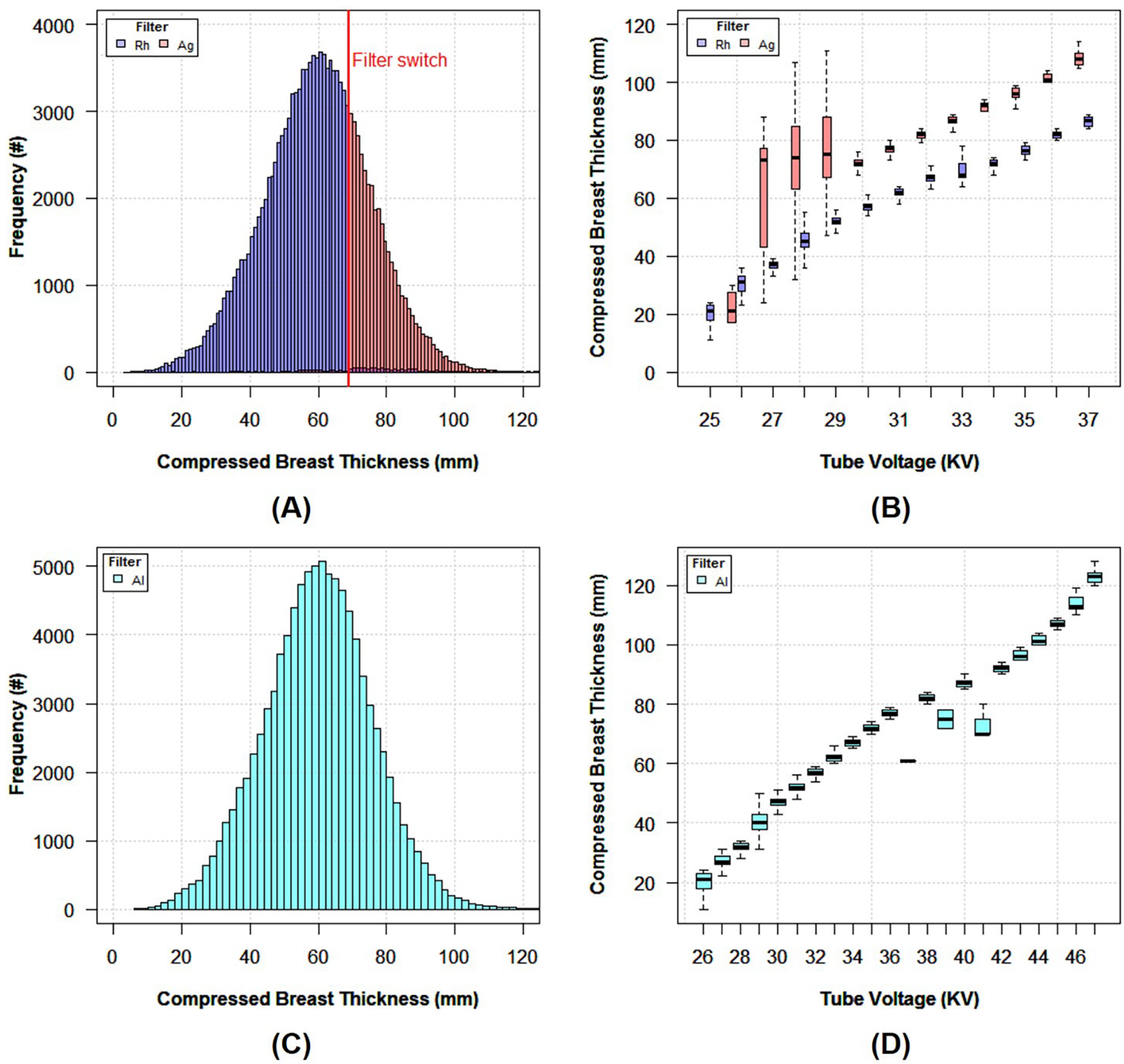

Fig. 7. (A) Frequency of images as a function of CBT, stratified by target-filter combination for DM. (B) Average CBT as a function of the kV applied across the X-ray tube for W/Rh and W/Ag as target-filter combination. (C) Frequency of images as a function of CBT for W/Al as target-filter combination. (D) Average CBT as a function of the kV applied across the X-ray tube for W/Al as target-filter combination.

exists ($r = 0.94$). ANOVA was calculated and it showed significant differences in a comparison of kV (p-value < 0.001).

For DBT, the W/Al target-filter combination is used exclusively (Fig. 7C). Thus, the only recourse is for the system to use higher kV to improve the X-ray penetration for thicker breasts (Fig. 7D). A strong positive correlation between CBT and kV exists ($r = 0.96$). ANOVA was also calculated and it showed significant differences in a comparison of kV (p-value < 0.001). Note that three kV (37, 39 and 41 kV) were almost never ($n = 6$) used in our group of 96,520 DBT images.

4.4. Average glandular dose

Exposure settings (e.g. target-filter combination, kV, mAs, etc.) and average glandular dose (AGD) vary depending upon patient breast thickness and composition. Table 3 shows that the average dose per image is 25.6% higher for DBT than DM. Note that the Selenia Dimensions can obtain a Tomo Combo study containing both DBT and DM images; here we are evaluating the system, so the dose from the DBT and DM portions of Tomo Combo studies are reported separately.

Using our tracking system, we can monitor the AGD reported by the manufacturer for different breast sizes. As expected, the AGD increases with breast thickness as shown in Fig. 8A. The error bars represent the standard deviation. A strong positive correlation between AGD and CBT is seen in both DM ($r = 0.61$) and DBT images ($r = 0.92$). Although we have an overall dose increase of 25.6% with the transition from DM to DBT, the differences in mean AGD vary with breast size, reaching 37%

Table 3
Summary of AGD and CBT categorized by breast view position for the DM and DBT modalities.

Modality	Breast View	No. Images	CBT, mm (avg ± SD)	AGD, mGy (avg ± SD)
DM	CC	63,046	56.6 ± 13.7	1.59 ± 0.64
	MLO	75,659	63.3 ± 16.6	1.90 ± 0.77
	CC & MLO	**138,705**	**60.2 ± 15.7**	**1.76 ± 0.73**
DBT	CC	47,981	57.2 ± 13.8	2.04 ± 0.65
	MLO	48,539	63.4 ± 17.1	2.38 ± 0.82
	CC & MLO	**96,520**	**60.3 ± 15.8**	**2.21 ± 0.76**

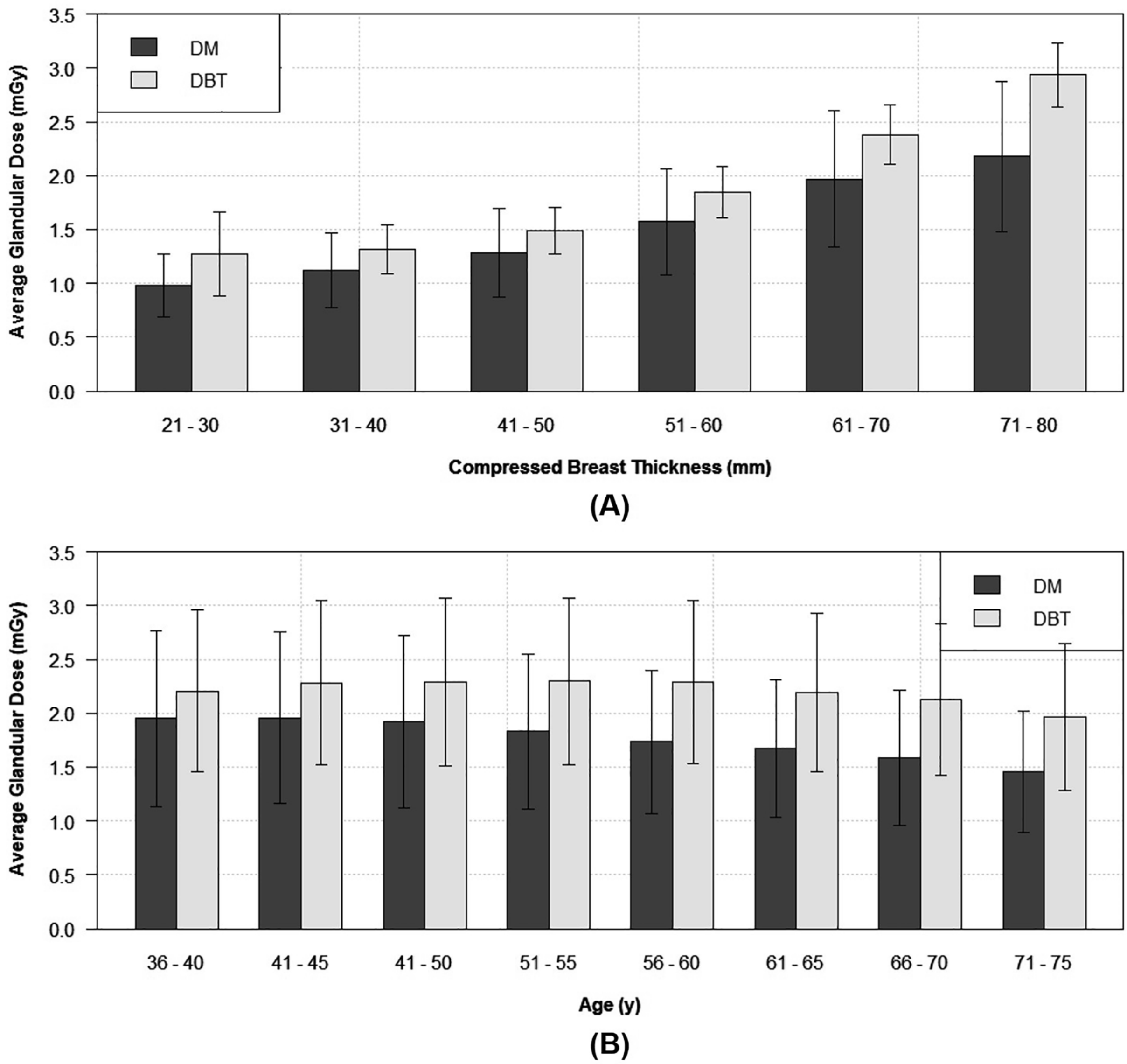

Fig. 8. AGD as a function of (A) CBT and (B) patient age for modalities DM and DBT.

for thick breasts (71–80 mm). There were significant differences in the pairwise comparison between the categorical variables (p-value < 0.001).

We also calculated the mean AGD by patient age (Fig. 8B). A weak negative correlation between AGD and patient age is seen in both DM ($r = -0.28$) and DBT images ($r = -0.16$). For the DM images, the mean AGD for older women (71–75 years old) is 35% less than for younger women (36–40 years old). For the DBT images, this difference is 13%. There were significant differences in the pairwise comparison between adjacent categorical variables (p-value < 0.001).

Using our tracking system, we can monitor the AGD in different mammography units as a function of CBT. Fig. 9 shows the mean AGD as a function of CBT, segregated by mammography unit (A-D). The reference dose (Fig. 9) is the average over the four units, thus the deviation of the data points from a line of unit slope will identify mammography units that produce more or less radiation than the average for the department. The error bars represent the standard error. Fig. 9A is for DM, and Fig. 9B is for DBT. Note that in Fig. 9A, the data closely follows the unit slope line to a dose of 2.0 mGy; above this dose the data deviate more from the unit slope line. This transition occurs when the Hologic systems AEC programming selects the Ag filter for thicker breasts. In the DBT mode, three of the four systems have dose performance that is nearly identical; one system provides dose approximately 5% higher than the others.

5. Discussion

The developed system successfully stored the metadata from each image in a short time (2.28 and 3.84 s on average to store each DM and DBT image, as shown in Table 2). The storage time per study varies because the number and size of images in each study varies. For example, some patients were imaged multiple times due to tiling or implants, and conversely some patients were imaged unilaterally. The transfer time (DIMSE C-MOVE) from PACS may vary as well, because of the priority that PACS associates to each DICOM SCP. DICOM DIMSE from imaging systems used in clinical practice have higher priority in the PACS, than DIMSE for our dose monitoring system. Given that the developed system was initially for research, we arranged that data transfer occurred outside of normal operating hours (12am - 5am), when clinical imaging and other high-priority jobs were not being performed to avoid impacting clinical operations. However, we have calculated that the impact on clinical practice would be minimal in our PACS environment even if the dosimetry information was sent at the time of study acquisition, because both our PACS and network

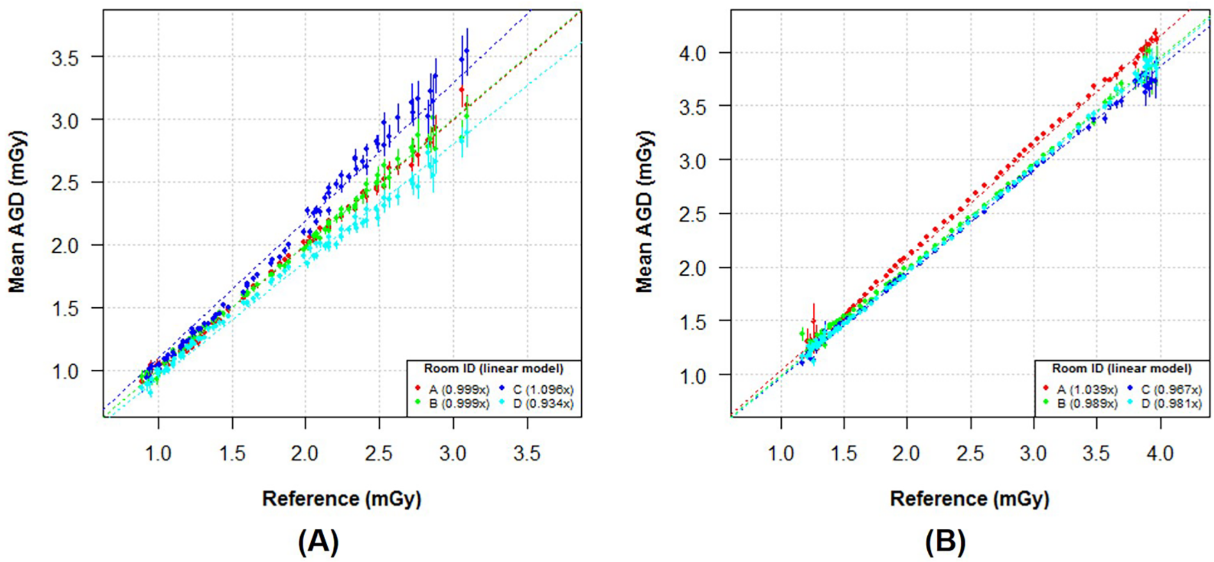

Fig. 9. Mean AGD matched by CBT as a function of mean AGD of four mammography units (A, B, C, and D). (A) Modality DM and (B) modality DBT.

infrastructure have spare bandwidth. The impact on other organizations would depend upon their PACS volume, and the capacity of their PACS and network. Queries to the BI client side application are in real-time, and do not impact the PACS since it is a distinct application, or the network since the data volume is small (see Fig. 1).

Although not presented here, our system can report data not just from a specific machine or from a specific patient population, but it can also report data by technologist. These data are useful in identifying trends in practice - such as variations in CBT or compression force. As an example, we found that 1755 (1.3%) DM images and 632 (0.7%) DBT images has a compression force higher than 200 N. They were considered outliers in the data analysis (Fig. 6B). This exceeds the maximum automatic compression force limit, and thus represents cases in which the technologist applied additional pressure after automatic compression was complete. These data can indicate patterns of use when stratified by technologist. It should be stressed that the Mammography Quality Standards Act (MQSA) states that the maximum compression force for the initial power drive shall be between 111N (25 lb) and 200N (45 lb) [17]. We also identified 421 (0.3%) DM images and 96 (0.1%) DBT images where there was no compression force information recorded. In our experience, these represent cases in which the compression force was below some minimum value. This value is machine dependent.

There is a clear trend that compression force varies with breast thickness; on average, larger breasts are imaged using higher compression force in our institution (Fig. 6C). We attribute this dependence to institutional practice guidelines. We cannot assure that other imaging centers will have similar trends. In addition, we noticed that the breast compression is also higher for MLO views than CC (Fig. 6D). We attribute this difference to the presence of the pectoralis muscle in the MLO view, which is less compressible than breast tissue.

In DM, the AEC for the Selenia Dimensions is set up to switch the target-filter combination from W/Rh to W/Ag at a CBT of 70 mm (Fig. 7A). However, our tracking system detected a small number of images (less than 1%) where the AEC selected the W/Rh for breasts thicker than 70 mm and W/Ag for breasts thinner than 70 mm. We cannot explain why the AEC selected unpredictable target-filter combinations to generate these images because we do not have access to the manufacturer AEC specifications. However, we know that the manufacturer determines the imaging settings based on estimated measurements of breast thickness and density. We believe that the breast density estimated by the manufacturer might be the determining factors to the AEC imaging settings of unpredictable target-filter combinations.

The tracking system can also show unexpected ‘features’ of the mammography units. For example, we found only 0.006% of the DBT images (6 out of 96,520) were acquired at 37, 39 or 41 kV (Fig. 7D). Again, we cannot explain the reason for this finding. However in DBT, the kV is determined primarily by breast thickness, thus we believe that those kV settings are assigned to only a small range of thicknesses.

Our dataset consists of DBT and DM screening exams acquired over eight years (2010-present). During this time, we have acquired images for screening mammography using various imaging modes: (1) DM-only – screening mammography using only DM images (2010), (2) DM-DBT – screening mammography using Tomo Combo (both DM and DBT) images (2011–2014), and (3) DBT-s2D – screening mammography using DBT and synthetic 2D images (2014-present). We have previously used our dose tracking system to compare the radiation dose to women in our screening population over these specific time intervals. [10–12,18,19] In this paper, we report the doses on a per machine, rather than per patient basis.

In our breast imaging center, we observe that DBT images resulted in a 25.6% higher dose than DM images (2.21 mGy vs. 1.76 mGy). This difference in not attributable to differences in the CBT between DM and DBT, as the CBT does not differ significantly (p-value = 0.27) between the two groups (Table 3). The measured dose increase differs from the typical dose increase reported by the manufacturer because the dose increase is typically reported for the ACR phantom. The dose increase we observed may differ from that reported at other sites because dose varies differently as a function of breast thickness for DM and DBT.

The average AGD is higher for MLO than the CC views (Table 3). The dose is 19.5% higher in DM and 16.7% higher in DBT. We attribute the higher radiation dose for the MLO views to the greater thickness of the breast in the MLO (average increase in thickness 6.7 mm for DM and 6.2 mm for DBT). The difference in CBT is due to the presence of the pectoralis muscle in the MLO images. Thicker breasts are exposed to a higher level of radiation dose (Fig. 8A). When comparing 71–80 mm thick breasts with 21–30 mm thick breasts, the dose increases by 118% for DM images and 130% for DBT images.

Breasts tend to become less dense as women get older, and thus the patient dose should decrease with age (Fig. 8B). This is especially true for women who have reached menopause (average age of onset at 51.3 years in United States) [20]. For women older than 51 years, we found that the mean AGD was reduced up to 30% and 25% for images acquired using DM and DBT, respectively. The differences in AGD were statistically significant (p-value < 0.001).

Our system can report and monitor radiation dose by mammography unit (Fig. 9). We observed that the mammography unit located in room C generates DM images using higher radiation dose levels than the average and room D generates DM images using lower radiation dose levels, in particular for thicker breasts (Fig. 9A).

It is important to remember that the doses reported here are calculated on a per image basis. Women who have large breasts sometimes need extra views (tiling), and women with suspicious findings and/or implants may also need additional views. Thus, it is not possible to equate machine performance directly with patient statistics. Previously, we used our dose tracking system to compare the radiation dose in our screening population [10–12,18,19].

This dose tracking system has been used in our diagnostic mammography environment since 2014. In a prior study [21], we calculated the total dose to patients in our diagnostic imaging population. We showed differences in AGD divided by finding types, including calcifications, masses, asymmetries, and architectural distortions. We analyzed radiation dose in two different time-points, before and after the implementation of DBT in our institution. We also compared radiation dose of DM and DBT guided stereotactic breast biopsies [22].

The accuracy of metadata information provided by the manufacturer is not covered in this paper. A better estimation of the AGD can be obtained if patient-specific breast density is considered. The SQL database implementation allows the metadata storage from external sources [10] to verify parameters such as, breast density, over and under exposures, over and under imaging processing, bad positioning, etc. We are currently using our tracking system to verify the accuracy of the radiation dose reported by the manufacturer.

We are also investigating the effect of radiation dose in the image quality of clinical mammograms. The image quality is evaluated using an anisotropic quality index, which assesses signal-difference-to-noise ratio and dose efficiency in DM and DBT [23–25]. In the future, we will include these image quality features in the radiation dose tracking system. It is important to stress that our dose tracking system is capable of tracking specific patient information to identify outliers, such as under and over exposures.

Although also not presented here, our dose tracking and reporting system supports the metadata storage of different vendors. We showed in previous publications the comparison of radiation dose using the Tomo Combo mode of different vendors [26]. We are currently conducting a multi-vendor and multi-site study using our dose tracking system [24].

6. Conclusion

The dose tracking system developed in this work provides different data visualizations for quality assurance of screening and clinical diagnostic procedures in radiology. The database model supports relational data processing and additional information from external sources can be integrated to assure the quality of the mammography systems. This system can report inconsistences in exposure factors for clinical practice and can highlight differences in the level of radiation dose by manufacturer, model, patient and technologist.

Acknowledgments

Funding for the research is supported by the following grants: CAPES 99999.014175/2013–04, NIH U54-CA163313-04 and ACRIN PA 4006.

References

[1] Cook TS, Zimmerman SL, Steingall SR, Maidment ADA, Kim W, Boonn WW. Informatics in radiology: RADIANCE: an automated, enterprise-wide solution for archiving and reporting CT radiation dose estimates. Radiographics 2011;31(7):1833–46. https://doi.org/10.1148/rg.317115048.
[2] Wang S, Pavlicek W, Roberts CC, Langer SG, Zhang M, Hu M, et al. An automated DICOM database capable of arbitrary data mining (Including Radiation Dose Indicators) for quality monitoring. J Digital Imaging 2011;24(2):223–33. https://doi.org/10.1007/s10278-010-9329-y.
[3] Shih G, Lu ZF, Zabih R, Kennedy D, Loftus M, Shih WJ, et al. Automated framework for digital radiation dose index reporting from CT dose reports. Am J Roentgenol 2011;197(5):1170–4. https://doi.org/10.2214/AJR.11.6650.
[4] Zhang M, Pavlicek W, Panda A, Langer SG, Morin R, Fetterly KA, et al. DICOM index tracker enterprise: advanced system for enterprise-wide quality assurance and patient safety monitoring 2015;9418:94180L–94180L–9. doi: 10.1117/12.2082120.
[5] Huda W, Vance A. Patient radiation doses from adult and pediatric CT. AJR Am J Roentgenol 2007;188(February):540–6. https://doi.org/10.2214/AJR.06.0101.
[6] Bogdanich, W. Radiation Overdoses Point Up Dangers of CT Scans. 2009. URL: http://www.nytimes.com/2009/10/16/us/16radiation.html.
[7] Verdun F, Schnyder P, Gutièrrez D, Gudinchet F. Patient dose optimization in pediatric computerized tomography. Rev Med Suisse 2006;2(73):1752–7.
[8] Albert GW, Glasier CM. Strategies for computed tomography radiation dose reduction in pediatric neuroimaging. Neurosurgery 2015;77(2):228–32. https://doi.org/10.1227/NEU.0000000000000764.
[9] Strauss KJ, Goske MJ, Morrison G. Image gently vendor summit: working together for better estimates of pediatric radiation dose from CT. Am J Roentgenol 2009;192:1169–75. https://doi.org/10.2214/AJR.08.2172.
[10] Barufaldi B, Maidment ADA, Cook T, Synnestvedt M, Conant E, Schnall M. A radiation dose reporting system for mammography and digital breast tomosynthesis. In: Radiological Society of North America. Chicago, USA.; 2014.
[11] Barufaldi B, Zuckerman S, Synnestvedt M, Connant E, Schnall M, Schiabel H, et al. Impact of 2D reconstructed mammograms on patient dose in the clinical practice of tomosynthesis. In: Radiological Society of North America Meeting. Chicago, USA.; 2015.
[12] Zuckerman SP, Conant EF, Keller BM, Maidment ADA, Barufaldi B, Weinstein SP, et al. Implementation of synthesized two-dimensional mammography in a population-based digital breast tomosynthesis screening. Radiol J 2016;000:1–7. https://doi.org/10.1148/radiol.2016160366.
[13] NEMA. DICOM PS3.8 2016d – Network Communication Support for Message Exchange. Tech. Rep.; Rosslyn, VA; 2016a.
[14] Pianykh OS. Digital Imaging and Communications in Medicine (DICOM): a practical introduction and survival guide. Berlin Heidelberg: Springer9783540745709; 2010.
[15] NEMA]. Digital imaging and communications in medicine (DICOM) Part 6: Data dictionary. Tech. Rep.; Rosslyn, VA; 2016b.
[16] Cohen J.. Statistical power analysis for the behavioral sciences. 1988. ISBN 0121790606. 1210.1833v2; https://doi.org/10.1234/12345678.
[17] Monsees BS. The Mammography Quality Standards Act: an overview of the regulations and guidance. Radiologic Clinics North Am 2000. https://doi.org/10.1016/S0033-8389(05)70199-8.
[18] Conant E, Oustimov A, Zuckerman S, McDonald E, Weinstein S, Maidment A, et al. Summary of outcomes from consecutive years of tomosynthesis screening at an American academic institution; vol. 9699. Springer International Publishing Switzerland; 2016. ISBN 9783319415451. https://doi.org/10.1007/978-3-319-41546-8_3.
[19] Barufaldi B, Mcdonald E, Conant E, Maidment A. Diagnostic radiation dose after the implementation of digital breast tomosynthesis screening. July. ISBN 9781510620070; 2018a, p. 49. doi: 10.1117/12.2318140.
[20] Mckinlay SM. The normal menopause transition. Maturitas 1992;4(14):103–15.
[21] Barufaldi B, McDonald E, Conant E, Maidment A. Diagnostic Radiation Dose after the Implementation of Digital Breast Tomosynthesis Screening. In: 14th International Workshop on Breast Imaging. Atlanta, USA.; 2018b, doi: 10.1117/12.2318140.
[22] Amir T, Barufaldi B, Zuckerman S, Maidment A, Conant E. Comparison Between Radiation Dose of 2D Digital versus Digital Tomosynthesis Guided Stereotactic Breast Biopsies: Tomosynthesis Wins! In: Radiological Society of North America Meeting. Atlanta, USA.; 2018.
[23] de Oliveira H, Barufaldi B, Borges L, Gabarda S, Bakic P, Maidment A, et al. Validation of no-reference image quality index for the assessment of digital mammographic images. In: SPIE Medical Imaging 2016. San Diego, USA.; 2016, doi: 10.1117/12.2217229.
[24] Barufaldi, B.. Radiation Dose Assessment in Mammography by Using a Computerized Dose Tracking System (translated to EN). Published in Universidade de Sao Paulo. Ph.D. thesis; 2016. URL: http://www.teses.usp.br/teses/disponiveis/18/18152/tde-22032016-153741/pt-br.php.
[25] Barufaldi B, Borges L, Bakic P, Vieira M, Schiabel H, Maidment A. Assessment of automatic exposure control performance in digital mammography using a no-reference anisotropic quality index. In: SPIE Medical Imaging 2017. Orlando, USA.; 2017, doi: 10.1117/12.2255629.
[26] Vicenti K, Szoakowski P, Barufaldi B, Maidment A. Dose delivered to patients between tomosynthesis and standard compression views in mammography. Am Roentgen Ray Society Meeting 2017:1.